Archaeol Anthropol Sci (2018) 10:415–429
DOI 10.1007/s12520-016-0359-3

ORIGINAL PAPER

Innovation and tradition in the fourth century mosaic of the *Casa delle Bestie Ferite* in Aquileia, Italy: archaeometric characterisation of the glass tesserae

Sarah Maltoni[1,2] · **Alberta Silvestri**[2,3]

Received: 13 May 2016 / Accepted: 13 July 2016 / Published online: 2 August 2016

Abstract The present paper focuses on the archaeometric characterisation of 38 glass tesserae of various colours from an in situ mosaic in Aquileia, Italy, dated to the second half of the fourth century AD. The examination of the textural, mineralogical and chemical features, conducted by means of a multi-methodological approach (optical microscopy (OM), scanning electron microscopy-energy dispersive X-ray spectroscopy (SEM-EDS), electron probe micro analysis (EPMA), X-ray diffraction (XRD) and Fibre Optic Reflectance Spectrophotometer (FORS)), has provided valuable insights into the changes in the production technology during the transition between the Roman and the Late Antique periods. The assemblage is heterogeneous, and each chromatic group is composed of tesserae produced with different base glasses and colouring/opacifying techniques, suggesting diverse supplies. A small group of tesserae shows strict links to the Roman tradition in terms of both base glass and colouring/opacifying techniques and was probably obtained by re-using tesserae from older mosaics. Conversely, a larger group of tesserae shows textural and chemical evidence of recycling and indicates the prompt use of "new" opacifying technologies (such as the use of tin compounds) or uncommon technological solutions (such as the use of quartz and bubbles as opacifiers or the addition of metallurgical slags in red tesserae), suggesting a specific production in the fourth century AD.

Keywords Mosaic tesserae · Glass · Roman period · Late Antiquity · Aquileia · Production technology

✉ Sarah Maltoni
sarah.maltoni@unipd.it

[1] Department of Cultural Heritage, piazza Capitaniato 3, 35139 Padova, Italy

[2] Department of Geosciences, via G. Gradenigo 6, 35131 Padova, Italy

[3] CNR, Istituto di Geoscienze e Georisorse, via G. Gradenigo 6, 35131 Padova, Italy

Introduction

The technology for producing opaque-coloured glass has been known since the Bronze Age in Mesopotamia and Egypt. However, in pre-Roman times, glass was considered a precious material and therefore reserved for beads or small, high-status objects (Newton and Davison 1989). During the Roman and Byzantine times, the glassmaking industry reached its peak of production. In the centuries between the first and the ninth AD, glass was used for several types of objects, from precious ornaments to very common tableware, and the presence of glass in mosaics and *opus sectile* became usual and widespread (Boschetti et al. 2008).

The glass-making and glass-colouring techniques of the pre-industrial world were strongly dependant on the accessibility of specific raw materials that were derived from a limited number of ores (see for instance Shortland 2002 for antimony; Shortland et al. 2006 for natron; Freestone 2008 for coastal sands in Roman glassmaking). Consequently, major geo-political changes could have a dramatic influence on the production.

The fourth century AD represents a period of change between Roman and Byzantine/Early Medieval glass technology due to the appearance of new glass compositions (Freestone 1994; Freestone et al. 2000) and the substitution of Sb-based technologies for glass-colouring and opacification with other types of compounds (Tite et al. 2008). Therefore, the investigation of a glass mosaic precisely dated to this transition period is a unique opportunity to

investigate how the change occurred in a specific area. In particular, the reception of the new technology and the persistence of old ones, the application of new or uncommon solutions to overcome the lack of certain raw materials, the re-use of previous tesserae and the extent of recycling can be effectively investigated via archaeometric characterisation of the glass tesserae. Furthermore, studying an in situ, well-dated mosaic from Aquileia is a rare opportunity that will shed light on the role of the city in the Antique and Late Antique world.

Site

The *Casa delle Bestie Ferite* (House of the Wounded Animals), which derives its name from the mosaic of hunting scenes on the floor of the main room, lies in the north-eastern part of the ancient city of Aquileia and had a surface area of approximately 800 m^2.

The site was partially investigated by L. Bertacchi between 1961 and 1962 (Bertacchi 1963) and has been the object of a systematic archaeological campaign by the Department of Archaeology (now Department of Cultural Heritage) of the University of Padova since 2007. The area, apparently peripheral with respect to the forum, was located in a strategic position and was bounded by the via Annia (an important road that connected Aquileia to the city of Padova) and the *cardus maximum* (Bueno et al. 2012).

Recent excavations revealed three main construction phases for the house between the late first and the mid-fourth century AD, when the House was completely restructured and a large and complex figurative mosaic was realised in the main room (Bueno and Centola 2014).

The mosaic represents a complex figurative composition comprising hunting scenes, wild animals, personifications of the seasons and other decorative motifs involving birds, vegetal and geometric patterns that frame the different figurative parts (Salvadori and Boschetti 2014). The mosaic employs a large quantity of stone tesserae, but glass and ceramic tesserae are also present, especially in the figurative scenes (Salvadori and Boschetti 2014). The stylistic and iconographic study of the mosaic identified the presence of several groups of workers and more than one master that worked at the same time. The various groups of mosaicists worked following a general project in the absence of a strong centralised control, which is reflected in mistakes in geometric patterns and inconsistencies (Salvadori and Boschetti 2014) not ascribable to different construction phases or restoration.

Materials

In total, 38 glass tesserae, representative of all the available colours, were chosen for archaeometric analyses. To preserve the mosaic as much as possible, detached tesserae were primarily sampled. In the case of colours available only in in situ tesserae (i.e. orange and red), micro-sampling was conducted. On the basis of their macroscopic appearances, samples were divided into seven colour macro-groups (i.e. blue, turquoise, white, green, yellow, red and colourless), which were further divided into various chromatic groups (Table 1), following, as much as possible, the colourimetric subdivision already applied to the glass tesserae of the St. Prosdocimus mosaic in Padova (Silvestri et al. 2011). Additionally, seven tesserae of the chromatic groups "dark blue", "turquoise", "gold" and "colourless" are translucent or transparent, i.e. no inclusion was intentionally employed to modify the transparency of the glass; all the other tesserae are opaque or semi-opaque due to various amounts of opacifiers in the glassy matrix.

For the full characterisation of the gold tessera, which is composed of two layers of clear colourless glass enclosing a gold leaf, both the supporting tessera (named BF AU1) and the *cartellina* (named BF AU1 cart) were sampled. Consequently, the number of the tesserae (38) does not correspond to the number of analytical samples (39).

Experimental

Taking into account that mosaic tesserae are complex artefacts composed of a glassy matrix in which crystals with various textures and functions are dispersed, a multi-methodological approach is required to fully characterise them. In the present study, textural analyses are carried out by means of optical microscopy (OM) and scanning electron microscopy (SEM). Using an energy-dispersive spectrometer (EDS) coupled with SEM, qualitative chemical analyses of both the glassy matrix and the inclusions are performed. Mineralogical analyses of the opacifiers and relic/newly formed phases and quantitative chemical analyses of the glassy matrix are carried out using X-ray diffraction (XRD) and an electron probe micro analysis (EPMA), respectively.

The OM observations were conducted under reflected light with a Nikon Eclipse ME600 microscope.

The scanning electron microscopy-energy dispersive X-ray spectroscopy (SEM-EDS) analyses were performed with an ESEM FEI Quanta Inspect equipped with an Oxford energy-dispersive spectrometer and an FEI Quanta 200 FEG-ESEM instrument equipped with a Genesys energy-dispersive X-ray spectrometer. In both instrumentations, SEM images were taken by collecting the backscattered electron signal (BSE), operating under high-vacuum conditions (<4 Pa) and with an accelerating voltage of 20–25 kV and a working distance of approximately 10 mm. The high-voltage conditions ensure good image contrast and allow the EDS chemical analyses to be conducted without changing the microscope conditions.

The instrument employed for the EPMA analyses was a CAMECA-SX50, equipped with four wavelength-dispersive

Table 1 Original chemical compositions (EPMA data, expressed as wt%) and standard deviation (in italics) of the glass samples from the mosaic of the *Casa delle Bestie Ferite* in Aquileia, grouped on the basis of the colour macro-group

Colour macro-group	Chromatic group	Sample	Diaphaneity	SiO_2	Na_2O	CaO	Al_2O_3	K_2O	MgO	MnO	Fe_2O_3	TiO_2	P_2O_5	SO_3	Cl	CoO	CuO	ZnO	SnO	Sb_2O_3	PbO	Tot
Turquoise	Dark blue	BF BS1	Translucent	66.08	20.02	7.30	1.96	0.29	1.00	0.85	0.64	0.11	0.07	0.35	1.52	<0.03	0.55	<0.04	<0.04	0.05	<0.08	100.79
				0.13	*0.14*	*0.11*	*0.06*	*0.01*	*0.03*	*0.08*	*0.03*	*0.03*	*0.02*	*0.02*	*0.04*		*0.03*			*0.02*		
	Turquoise	BF TU TR1	Translucent	68.45	16.50	7.86	2.68	0.60	0.63	1.05	0.51	0.07	0.07	0.25	1.01	<0.03	1.01	<0.04	<0.04	<0.04	<0.08	100.69
				0.35	*0.33*	*0.04*	*0.10*	*0.03*	*0.03*	*0.05*	*0.02*	*0.03*	*0.01*	*0.02*	*0.03*		*0.07*					
		BF TU1	Opaque	66.35	17.95	3.89	2.13	0.44	0.64	<0.05	1.09	0.15	<0.05	0.36	1.15	<0.03	4.13	0.07	0.27	1.62	0.09	100.34
				0.48	*0.20*	*0.07*	*0.08*	*0.04*	*0.02*		*0.08*	*0.02*		*0.03*	*0.04*		*0.11*	*0.02*	*0.02*	*0.25*	*0.06*	
	Aquamarine	BF AQ1	Semiopaque	65.26	19.99	6.16	2.38	0.38	1.02	0.41	0.74	0.14	0.07	0.32	1.65	<0.03	1.36	<0.04	0.07	<0.04	0.34	100.29
				0.43	*0.17*	*0.09*	*0.10*	*0.04*	*0.05*	*0.03*	*0.06*	*0.02*	*0.02*	*0.03*	*0.03*		*0.02*		*0.02*		*0.05*	
		BF AQ2	Semiopaque	65.74	19.98	6.17	2.32	0.36	1.02	0.42	0.75	0.15	0.07	0.29	1.64	<0.03	1.35	<0.04	0.06	<0.04	0.37	100.68
				0.27	*0.34*	*0.09*	*0.11*	*0.05*	*0.03*	*0.05*	*0.06*	*0.02*	*0.01*	*0.02*	*0.04*		*0.04*		*0.02*		*0.04*	
	Pale blue	BF CE1	Opaque	65.97	14.64	7.43	2.85	0.74	0.75	1.12	0.88	0.11	0.11	0.38	0.62	<0.03	1.41	<0.04	0.13	3.17	0.10	100.40
				1.16	*0.38*	*0.12*	*0.21*	*0.06*	*0.02*	*0.08*	*0.05*	*0.03*	*0.04*	*0.03*	*0.02*		*0.06*		*0.03*	*1.28*	*0.04*	
		BF CE2	Semiopaque	67.83	18.69	5.68	3.22	0.40	0.90	0.13	0.59	0.12	<0.05	0.37	1.44	<0.03	0.86	<0.04	0.10	<0.04	0.13	100.47
				0.50	*0.36*	*0.06*	*0.10*	*0.05*	*0.03*	*0.04*	*0.06*	*0.02*		*0.33*	*0.17*		*0.05*		*0.02*		*0.06*	
	Pale green	BF VCH1	Semiopaque	66.57	19.07	6.07	2.89	0.40	0.97	0.35	0.78	0.14	0.04	0.28	1.51	<0.03	0.42	<0.04	0.09	<0.04	0.38	99.95
				0.64	*0.41*	*0.05*	*0.07*	*0.05*	*0.03*	*0.03*	*0.06*	*0.01*	*0.02*	*0.02*	*0.04*		*0.02*		*0.03*		*0.06*	
		BF VCH2	Semiopaque	68.03	18.92	5.84	2.97	0.41	0.92	0.16	0.59	0.12	<0.05	0.28	1.46	<0.03	0.45	<0.04	0.05	<0.04	<0.08	100.26
				0.35	*0.35*	*0.07*	*0.09*	*0.02*	*0.03*	*0.03*	*0.05*	*0.02*		*0.03*	*0.05*		*0.03*		*0.02*		*0.04*	
		BF VCH3	Semiopaque	66.87	18.13	6.68	2.19	0.50	0.87	0.46	0.72	0.10	<0.05	0.32	1.26	<0.03	0.78	<0.04	0.06	0.60	0.35	99.90
				0.57	*0.19*	*0.13*	*0.11*	*0.03*	*0.05*	*0.05*	*0.09*	*0.01*		*0.03*	*0.03*		*0.05*		*0.02*	*0.06*	*0.08*	
Green	Green	BF VP1	Opaque	59.23	16.50	6.00	1.96	0.39	0.99	0.56	1.16	0.13	0.05	0.21	1.36	<0.03	1.80	<0.04	0.65	<0.04	8.81	99.81
				0.48	*0.29*	*0.22*	*0.10*	*0.04*	*0.04*	*0.02*	*0.09*	*0.03*	*0.02*	*0.03*	*0.04*		*0.09*		*0.32*		*0.63*	
		BF VP2	Opaque	61.55	18.00	6.44	1.94	0.36	0.99	0.24	1.04	0.15	0.05	0.21	1.59	<0.03	1.58	<0.04	0.45	0.13	5.50	100.20
				0.46	*0.28*	*0.11*	*0.11*	*0.03*	*0.04*	*0.03*	*0.03*	*0.01*	*0.02*	*0.03*	*0.02*		*0.03*		*0.11*	*0.02*	*0.29*	
		BF VP3	Opaque	60.38	17.05	5.83	2.07	0.49	0.97	0.67	1.35	0.16	0.09	0.20	1.44	<0.03	1.43	<0.04	0.37	0.09	6.90	99.48
				0.61	*0.30*	*0.08*	*0.08*	*0.02*	*0.03*	*0.04*	*0.14*	*0.02*	*0.05*	*0.03*	*0.08*		*0.08*		*0.11*	*0.02*	*0.36*	
		BF VP4	Opaque	58.67	17.15	5.80	1.99	0.38	0.90	0.96	0.97	0.12	0.05	0.22	1.34	<0.03	2.99	<0.04	0.60	<0.04	8.32	100.47
				0.18	*0.23*	*0.12*	*0.10*	*0.05*	*0.03*	*0.04*	*0.05*	*0.02*	*0.02*	*0.04*	*0.05*		*0.09*		*0.17*		*0.24*	
	Dark green	BF VS1	Translucent	65.72	18.58	7.27	2.23	0.58	0.88	1.28	1.42	0.11	0.16	0.25	1.45	<0.03	0.90	0.16	<0.04	<0.04	<0.08	100.99
				0.31	*0.10*	*0.09*	*0.03*	*0.06*	*0.03*	*0.04*	*0.04*	*0.02*	*0.02*	*0.02*	*0.05*		*0.02*	*0.03*				
		BF VS2	Opaque	62.83	18.10	6.38	2.05	0.49	0.93	0.67	1.24	0.14	0.08	0.23	1.49	<0.03	2.16	<0.04	0.33	<0.04	3.61	100.73
				1.47	*0.19*	*0.25*	*0.09*	*0.06*	*0.03*	*0.08*	*0.16*	*0.03*	*0.02*	*0.04*	*0.06*		*0.10*		*0.28*		*0.85*	
Yellow	Yellow	BF GSO1	Opaque	65.63	17.50	5.88	1.90	0.47	0.52	0.31	0.45	0.07	<0.05	0.27	1.25	<0.03	0.03	<0.04	<0.04	0.55	5.16	99.99
				0.87	*0.29*	*0.05*	*0.09*	*0.04*	*0.02*	*0.01*	*0.05*	*0.01*		*0.03*	*0.03*		*0.02*			*0.12*	*0.81*	

Table 1 (continued)

Colour macro-group	Chromatic group	Sample	Diaphaneity	SiO_2	Na_2O	CaO	Al_2O_3	K_2O	MgO	MnO	Fe_2O_3	TiO_2	P_2O_5	SO_3	Cl	CoO	CuO	ZnO	SnO	Sb_2O_3	PbO	Tot
		BF GSO2	Opaque	63.69	16.60	4.56	1.96	0.60	0.58	0.42	1.28	0.13	0.06	0.37	0.87	<0.03	<0.03	<0.04	0.04	1.24	7.34	99.74
				0.74	*0.26*	*0.08*	*0.03*	*0.02*	*0.02*	*0.05*	*0.01*	*0.22*	*0.04*	*0.03*	*0.02*				*0.03*	*0.16*	*0.46*	
		BF GSO3	Opaque	66.03	17.66	4.49	2.12	0.57	0.70	0.59	1.38	0.16	0.07	0.32	1.04	<0.03	<0.03	<0.04	0.08	1.00	3.62	99.83
				1.25	*0.45*	*0.16*	*0.10*	*0.05*	*0.13*	*0.08*	*0.44*	*0.03*	*0.03*	*0.09*	*0.07*				*0.06*	*0.29*	*1.32*	
		BF GSO4	Opaque	54.93	15.56	5.22	1.93	0.45	0.59	0.95	0.74	0.17	<0.05	0.18	1.10	<0.03	<0.03	<0.04	1.73	<0.04	16.33	99.87
				0.74	*0.36*	*0.08*	*0.10*	*0.03*	*0.02*	*0.05*	*0.02*	*0.04*		*0.02*	*0.05*				*0.26*		*0.94*	
	Yellow green	BF VG1	Opaque	63.84	18.84	5.82	2.06	0.50	0.96	1.09	1.93	0.13	<0.05	0.27	1.30	<0.03	0.04	<0.04	0.23	<0.04	2.84	99.84
				1.34	*0.45*	*0.09*	*0.12*	*0.06*	*0.03*	*0.06*	*0.19*	*0.02*		*0.03*	*0.03*		*0.02*		*0.04*		*0.15*	
Blue	Azure	BF AZ1	Semiopaque	65.06	20.23	6.39	2.31	0.40	1.02	0.69	0.95	0.15	0.09	0.32	1.73	<0.03	0.15	<0.04	0.32	<0.04	0.73	100.54
				0.18	*0.16*	*0.04*	*0.06*	*0.03*	*0.04*	*0.04*	*0.06*	*0.01*	*0.01*	*0.03*	*0.07*		*0.03*		*0.01*		*0.09*	
		BF AZ2	Semiopaque	66.72	18.41	6.96	2.10	0.58	0.85	0.63	0.83	0.09	0.12	0.31	1.30	0.03	0.38	<0.04	<0.04	1.06	0.25	100.61
				0.12	*0.30*	*0.04*	*0.08*	*0.02*	*0.02*	*0.04*	*0.06*	*0.01*	*0.03*	*0.04*	*0.07*	*0.01*	*0.05*			*0.19*	*0.01*	
		BF AZ3	Semiopaque	66.84	18.63	6.80	2.09	0.48	0.79	0.63	0.85	0.10	0.12	0.33	1.36	0.05	0.14	<0.04	<0.04	0.96	0.30	100.47
				0.30	*0.26*	*0.06*	*0.11*	*0.04*	*0.03*	*0.05*	*0.06*	*0.02*	*0.01*	*0.04*	*0.03*	*0.01*	*0.02*			*0.03*	*0.04*	
		BF AZ4	Opaque	67.72	15.82	6.16	2.53	0.70	0.69	0.61	0.91	0.09	0.14	0.34	0.91	0.08	0.17	<0.04	<0.04	3.02	0.23	100.12
				0.45	*0.32*	*0.04*	*0.11*	*0.04*	*0.02*	*0.05*	*0.06*	*0.02*	*0.03*	*0.13*	*0.06*	*0.02*	*0.02*			*0.23*	*0.05*	
		BF AZ5	Semiopaque	66.89	16.49	7.03	2.29	0.59	0.76	0.61	1.08	0.08	0.18	0.36	0.99	<0.03	0.09	<0.04	<0.04	2.38	0.24	100.04
				0.31	*0.15*	*0.07*	*0.15*	*0.05*	*0.03*	*0.02*	*0.07*	*0.02*	*0.02*	*0.03*	*0.03*		*0.02*			*0.14*	*0.06*	
	Blue	BF B1	Opaque	67.62	16.42	5.94	2.32	0.67	0.65	0.61	0.95	0.10	0.16	0.35	0.85	0.08	0.16	<0.04	<0.04	3.03	0.23	100.13
				0.50	*0.16*	*0.07*	*0.10*	*0.05*	*0.02*	*0.03*	*0.03*	*0.03*	*0.03*	*0.03*	*0.05*	*0.02*	*0.03*			*0.12*	*0.06*	
White	Grey	BF GR1	Opaque	67.28	17.72	6.62	2.14	0.57	0.89	0.42	0.71	0.09	0.11	0.36	1.16	<0.03	0.08	<0.04	<0.04	1.83	0.14	100.12
				0.21	*0.38*	*0.05*	*0.05*	*0.03*	*0.03*	*0.02*	*0.07*	*0.03*	*0.02*	*0.04*	*0.03*		*0.02*			*0.16*	*0.03*	
Red	Orange	BF AV1	Opaque	37.27	7.14	7.30	3.87	0.87	1.31	0.15	2.73	0.37	0.35	0.16	0.38	<0.03	5.97	0.19	0.99	0.45	31.33	100.83
				0.14	*0.18*	*0.12*	*0.08*	*0.06*	*0.03*	*0.03*	*0.07*	*0.03*	*0.03*	*0.03*	*0.03*		*1.20*	*0.03*	*0.04*	*0.04*	*0.76*	
	Brown	BF M1	Opaque	64.37	19.42	6.30	2.01	0.46	0.90	1.28	4.21	0.13	<0.05	0.27	1.40	<0.03	0.46	0.07	<0.04	<0.04	0.08	101.35
				0.23	*0.19*	*0.10*	*0.09*	*0.03*	*0.02*	*0.07*	*0.02*	*0.03*		*0.04*	*0.03*		*0.17*	*0.01*				
		BF M2	Opaque	64.22	18.57	6.54	2.12	0.75	0.88	1.27	4.69	0.14	<0.05	0.24	1.27	<0.03	0.62	0.07	<0.04	<0.04	<0.08	101.41
				0.40	*0.44*	*0.04*	*0.03*	*0.05*	*0.03*	*0.05*	*0.17*	*0.02*		*0.03*	*0.04*		*0.17*	*0.02*			*0.05*	
		BF M3	Opaque	60.66	14.17	9.32	1.93	2.47	2.21	0.50	3.19	0.13	0.91	0.34	0.77	<0.03	1.95	0.06	0.22	0.42	1.33	100.58
				0.25	*0.15*	*0.07*	*0.10*	*0.10*	*0.05*	*0.05*	*0.03*	*0.12*	*0.03*	*0.04*	*0.10*		*0.32*	*0.03*	*0.02*	*0.03*	*0.08*	
		BF M4	Opaque	64.72	18.91	6.62	2.14	0.81	0.90	1.34	3.24	0.14	<0.05	0.26	1.30	<0.03	0.75	0.13	<0.04	<0.04	0.09	101.35
				0.32	*0.48*	*0.20*	*0.10*	*0.05*	*0.03*	*0.07*	*0.29*	*0.02*		*0.02*	*0.03*		*0.32*	*0.06*			*0.06*	
	Red	BF R1	Opaque	61.70	14.94	6.98	2.40	0.57	0.64	0.86	2.87	0.09	0.11	0.22	1.10	<0.03	1.19	<0.04	0.25	0.28	5.68	99.87
				0.35	*0.21*	*0.07*	*0.09*	*0.04*	*0.03*	*0.02*	*0.02*	*0.11*	*0.02*	*0.03*	*0.04*				*0.03*	*0.15*	*0.15*	
Colourless	Gold	BF AU1	Transparent	67.63	18.60	7.28	2.10	0.49	1.00	0.63	0.69	0.11	0.05	0.31	1.29	<0.03	<0.03	<0.04	<0.04	0.15	<0.08	100.33

Table 1 (continued)

Colour macro-group	Chromatic group	Sample	Diaphaneity	SiO_2	Na_2O	CaO	Al_2O_3	K_2O	MgO	MnO	Fe_2O_3	TiO_2	P_2O_5	SO_3	Cl	CoO	CuO	ZnO	SnO	Sb_2O_3	PbO	Tot
				0.47	*0.24*	*0.09*	*0.09*	*0.06*	*0.02*	*0.05*	*0.05*	*0.02*	*0.02*	*0.03*	*0.01*					*0.04*		
		BF AU1cart	Transparent	67.98	18.44	7.42	1.98	0.57	1.07	0.69	0.74	0.12	<0.05	0.30	1.25	<0.03	<0.03	<0.04	<0.04	0.15	<0.08	100.71
				0.15	*0.12*	*0.16*	*0.08*	*0.07*	*0.03*	*0.05*	*0.02*	*0.01*		*0.01*	*0.03*					*0.02*		
	Colourless	BF TR INC1	Transparent	72.42	15.73	7.07	2.37	0.52	0.45	0.14	0.35	0.05	0.11	0.12	1.15	<0.03	<0.03	<0.04	<0.04	<0.04	<0.08	100.48
				0.29	*0.20*	*0.07*	*0.13*	*0.02*	*0.01*	*0.04*	*0.03*	*0.04*	*0.02*	*0.04*	*0.02*							
		BF TR INC2	Transparent	67.20	19.09	7.09	1.96	0.53	0.93	0.68	0.73	0.12	<0.05	0.36	1.28	<0.03	<0.03	<0.04	<0.04	0.15	<0.08	100.12
				0.37	*0.43*	*0.06*	*0.08*	*0.05*	*0.04*	*0.03*	*0.02*	*0.05*		*0.03*	*0.05*					*0.01*		
		BF TR INC3	Transparent	67.90	19.41	6.36	2.07	0.38	0.76	0.96	0.52	0.10	0.07	0.28	1.59	<0.03	<0.03	<0.04	<0.04	0.05	<0.08	100.44
				0.81	*0.52*	*0.33*	*0.27*	*0.03*	*0.07*	*0.08*	*0.03*	*0.03*	*0.02*	*0.02*	*0.10*					*0.04*		

Chromatic group and diaphaneity also reported for each sample

spectrometers (WDS). The operating conditions were 20 kV and 2 nA for Na, Al, Si and K and 20 kV and 30 nA for Ca, Mn, Fe, Mg, Ti, S, Cl, P, Co, Cu, Sn, Sb, Pb and Zn, with a focused beam of 1 μm. Details on the analytical conditions and instrumental parameters have been recently published (Silvestri et al. 2015). Averages and standard deviations were calculated by measuring 6 analytical points on translucent tesserae and 12 points on opaque tesserae, avoiding inclusions.

The XRD analyses were performed using two instruments. One was a PANalytical X'Pert PRO diffractometer (Bragg-Brentano geometry), equipped with a Cu X-ray tube (40 kV and 40 mA) and X'Celerator detector. Scans were collected in the angular range 3–80° 2θ with a 0.03° virtual step size and a 100 s/step counting time. The other was a prototype consisting of an Agilent Supernova goniometer equipped with an X-ray micro-source assembled with a Pilatus 200K Dectris detector. The micro-X-ray source, MoKα, operates at 50 kV and 0.8 mA, with a spot size of 0.11 mm. The sample-to-detector distance was 68 mm. Data were collected in micro-X-ray powder diffraction mode, due to the polycrystalline nature of the samples. A detailed description of the instrument and instrumental parameters have been recently published (Angel and Nestola 2016; Nestola et al. 2016).

To obtain information on the colouring ions in selected glass tesserae, reflectance spectra were acquired. The instrument used was an Ocean Optics Fibre Optic Reflectance Spectrophotometer (FORS), which consisted of a light source, an integrating sphere and a spectrometer, all connected by means of optical fibres. The light source was a deuterium-halogen lamp (DH-2000), generating radiation between 210 and 1500 nm, and the spectrometer was a wavelength-dispersive system, mod. HR 2000+. The FORS spectra of the samples were acquired between 188 and 1100 nm, with 10 replicas and an acquisition time of 60 s.

The OM, SEM-EDS and EPMA analyses were performed on polished sections (for whole tesserae) and resin blocks (for micro-fragments). The polished sections were obtained by using a diamond-coated saw to cut layers approximately 500-μm thick. The cuts were perpendicular to the surface for tesserae with homogeneous textures and along the most representative direction for tesserae with banded textures. These layers were then mounted in epoxy resin and thinly sectioned to a thickness of ~100 μm. The micro-samples were entirely embedded in epoxy resin blocks. The surface of each thin section and resin block was then polished with a series of diamond pastes down to 0.02 μm grade and coated with conductive carbon film (only for EPMA and SEM-EDS). The XRD and FORS analyses were directly performed on the whole tesserae or micro-fragments for conservative purposes. In the FORS analyses, the glass tesserae were also flattened and polished with a series of diamond pastes up to 5 μm in order to guarantee maximum reflectance.

Results and Discussion

Despite the precise dating and short life of the mosaic of the *Casa delle Bestie Ferite* in Aquileia, the assemblage studied here is not homogenous, and each colour macro-group is composed of tesserae with different compositions, textures and colouring/opacifying techniques, as summarised in Table 2. In the present section, the results obtained on the Aquileia samples are presented and discussed with respect to two factors: the glassy matrix,

Table 2 Summary of the chemical, textural and mineralogical characteristics of the glass tesserae from the mosaic of the *Casa delle Bestie Ferite* in Aquileia

Colour macro-group	Sample	Diaphaneity	Chromatic group	Glassy matrix	Chromofore/ decolouriser	Opacifier/pigment	Additional information
Turquoise	BF BS1	Translucent	Dark blue	N	Copper	*None*	
	BF TU TR1	Translucent	Turquoise	N	Copper	*None*	
	BF TU1	Opaque	Turquoise	N	Copper	Ca-antimonates	
	BF AQ1	Semiopaque	Aquamarine	N	Copper	Quartz and bubbles	Sporadic Sn-oxide
	BF AQ2	Semiopaque	Aquamarine	N	Copper	Quartz and bubbles	
	BF CE1	Opaque	Pale blue	N	Copper	Ca-antimonates	
	BF CE2	Semiopaque	Pale blue	N	Copper	Quartz and bubbles	
	BF VCH1	Semiopaque	Pale green	N	Copper	Quartz and bubbles	
	BF VCH2	Semiopaque	Pale green	N	Copper	Quartz and bubbles	
	BF VCH3	Semiopaque	Pale green	N	Copper	Quartz and bubbles	+ Ca-antimonates
Green	BF VP1	Opaque	Green	N	Copper	Pb-stannate	
	BF VP2	Opaque	Green	N	Copper	Pb-stannate	
	BF VP3	Opaque	Green	N	Copper	Pb-stannate	
	BF VP4	Opaque	Green	N	Copper	Pb-stannate	
	BF VS1	Translucent	Dark green	N	Copper	*None*	
	BF VS2	Opaque	Dark green	N	Copper	Pb-stannate	
Yellow	BF GSO1	Opaque	Yellow	N		Pb-antimonate	
	BF GSO2	Opaque	Yellow	N		Pb-antimonate	
	BF GSO3	Opaque	Yellow	N		Pb-antimonate	
	BF GSO4	Opaque	Yellow	N		Pb-stannate	
	BF VG1	Opaque	Yellow green	N		Pb-stannate	
Blue	BF AZ1	Semiopaque	Azure	N	Cobalt	Quartz and bubbles	+ Sn-oxide and sporadic Ca-antimonates
	BF AZ2	Semiopaque	Azure	N	Cobalt	Quartz and bubbles	+ Ca-antimonates
	BF AZ3	Semiopaque	Azure	N	Cobalt	Quartz and bubbles	+ Ca-antimonates
	BF AZ4	Opaque	Azure	N	Cobalt	Ca-antimonates	
	BF AZ5	Semiopaque	Azure	N	Cobalt	Quartz and bubbles	+ Ca-antimonates
	BF B1	Opaque	Dark blue	N	Cobalt	Quartz and bubbles	+ Ca-antimonates
White	BF GR1	Opaque	Grey	N		Ca-antimonates	
Red	BF AV1	Opaque	Orange	N/A		Cuprite	
	BF M1	Opaque	Brown	N		Metallic copper	Metallurgical slag inclusion
	BF M2	Opaque	Brown	N		Metallic copper	
	BF M3	Opaque	Brown	A		Metallic copper	Metallurgical slag inclusion
	BF M4	Opaque	Brown	N		Metallic copper	Metallurgical slag inclusion
	BF R1	Opaque	Red	N		Metallic copper	
Colourless	BF AU1	Transparent	Colourless/gold	N	Sb-Mn	*None*	Gold foil
	BF AU1cart	Transparent	Colourless/gold	N	Sb-Mn	*None*	*Cartellina*
	BF TR INC1	Transparent	Colourless	N	*None*	*None*	
	BF TR INC2	Transparent	Colourless	N	Sb-Mn	*None*	
	BF TR INC3	Transparent	Colourless	N	Sb-Mn	*None*	

N natron, *A* ash, *N/A* natron/ash

with particular attention to the base glass employed, and the colouring/opacifying agents.

Glassy matrix

The chemical analyses performed by means of EPMA on the glassy matrices of the tesserae from Aquileia provided the opportunity to examine these complex artefacts from different perspectives. The original composition, reported in Table 1, provides useful information on the colouring and opacification processes (see the next sub-section for more details). However, to investigate the composition of the base glass employed, a "reduced" composition is calculated (Table 3) by subtracting the intentionally added elements (Pb, Cu, Sn, Sb, Mn and Zn), following the method described by Silvestri et al. (2014).

Judging by the reduced data for MgO and K_2O, most of the samples have contents of both oxides below 1.5 wt% (Table 3 and Fig. 1a), indicating that natron was used as the flux, in accordance with the Roman and Late Antique tradition. Exceptions include the brown BF M3, which exceeds the given compositional limits and is quite consistent with the use of a sodic plant ash as the flux, and the orange BF AV1, which falls into an intermediate field between natron and sodic plant ash. These two samples also exhibit high concentrations of phosphorous oxide and lime and low concentrations of chlorine with respect to the other samples (Table 3). These particular chemical features have already been observed in other red and orange tesserae dated to the Roman and Byzantine times (e.g. Gliozzo et al. 2008; Schibille et al. 2012; Gliozzo et al. 2012; Silvestri et al. 2014; Silvestri et al. 2015) and appear to be related to the colouring and/or opacifying of the glass, rather than to any differences in base glass composition. Charcoal and fuel ashes are sometimes hypothesised to have been used as internal reducing agents in the production of red and orange colours. This practise, also supported by analytical and experimental studies (Cable and Smedley 1987; Freestone 1987; Schibille et al. 2012), would explain the plant ash appearance of some red and orange tesserae. However, it should be noted that when vegetal/fuel ash is used as both the flux and reducing agent, as is the case with the brown tesserae BF M3 included in the plant ash compositional field, it becomes difficult to distinguish between the contribution of the flux and that of the internal reducing agent. In addition, the reduced composition of the orange sample BF AV1, with low soda and very high lime and alumina contents (Table 3), does not fit with the reference compositional groups for Roman and Byzantine times. This is probably due to the very high lead content of the present sample (equal to 31.3 wt% as PbO, Table 1), which strongly affects the reduced composition. Therefore, taking into account that the orange tesserae usually feature very high lead contents and that lead may play different roles in glassmaking (flux, enhancer of the refractive index, internal reducing agent and network former), it is possible that this specific coloured glass is a product of a primary batch originally containing lead.

Examining the natron samples on the basis of reduced magnesia, potash and soda, they can be divided into two groups, although the distinction is not neat: one, named BF1, contains comparably low concentrations of magnesia and potash and a generally lower soda concentrations ($15 > Na_2O > 18$ wt%), and the other, BF2, comprises the majority of the samples and the widest range of shades and is characterised by high magnesia and low potash concentrations and generally high soda concentrations (>18 wt%) (Fig. 1b and Table 3). Despite these differences, the two groups are relatively homogenous in terms of other reduced elements: alumina varies between 2 and 3.3 wt%, lime generally varies between 5 and 7 wt% and phosphorous oxide is below 0.2 wt% but seldom below the EPMA detection limits (0.05 wt%), as expected for natron-based glass (Table 3). In the binary diagram reduced soda vs. magnesia (Fig. 1b), four samples of BF1 appear closer to BF2: they are three yellow tesserae (BF GSO1, 2, 3) and one turquoise (BF TU1). Despite the high soda, which is one of the characteristics of BF2, the three yellow samples have comparable levels of potash and magnesia and for this reason are included in BF1. Differently, BF TU1 is a doubtful case: the opacifying technique (see next subsection) may have affected strongly the lime content of the base glass, which is not fully interpretable. Given the absence of detectable manganese, which is very frequent in the fourth century compositions, and the early Roman opacification technique identified, BF TU1 is included in BF1 although with some reserves.

Group BF1 is comparable to the Roman reference groups (see, for instance, the "Roman" composition reported in Nenna et al. 2000), although the absence of antimony and manganese in the reduced compositions limits more precise comparisons.

Group BF2 is not particularly consistent with any Roman or Late Antique reference group reported in the literature, such as, for instance, HIMT (Freestone 1994) or Levantine 1 (Freestone et al. 2000). The particularly high MgO content, typical of this group, may suggest several cycles of recycling and re-melting or prolonged secondary working (Paynter 2008; Paynter et al. 2015). However, in that case, the potash content is also expected to increase, and this is not the case for the BF2 tesserae, which generally feature low K_2O contents (below 0.5 wt%). The chemical features of group BF2 (high soda, high magnesia) are somewhat indicative of HIMT glass that has been diluted with "Roman" compositions, alongside a

Table 3 Reduced chemical compositions of all the glass samples from the *Casa delle Bestie Ferite* mosaic

Colour macro-group	Chromatic group	Sample	Group	SiO_2 red	Na_2O red	CaO red	Al_2O_3 red	K_2O red	MgO red	FeO red	TiO_2 red	P_2O_5 red	SO_3 red	Cl red	Tot
Turquoise	Dark blue	BF BS1	BF2	67.04	20.31	7.41	1.99	0.29	1.02	0.65	0.12	0.08	0.35	1.54	100.79
	Turquoise	BF TU TR1	BF1	69.88	16.84	8.03	2.73	0.61	0.64	0.52	0.08	0.08	0.26	1.03	100.69
		BF TU1	BF1	70.71	19.13	4.15	2.27	0.47	0.69	1.16	0.13	0.03	0.38	1.22	100.34
	Aquamarine	BF AQ1	BF2	66.72	20.44	6.30	2.44	0.38	1.05	0.76	0.12	0.07	0.32	1.68	100.29
		BF AQ2	BF2	67.23	20.43	6.31	2.37	0.37	1.05	0.77	0.12	0.08	0.29	1.68	100.68
	Pale blue	BF CE1	BF1	70.10	15.55	7.90	3.02	0.79	0.80	0.94	0.11	0.12	0.41	0.66	100.40
		BF CE2	BF2	68.64	18.91	5.75	3.26	0.40	0.91	0.60	0.12	0.03	0.37	1.46	100.47
	Pale green	BF VCH1	BF2	67.42	19.31	6.15	2.93	0.40	0.98	0.79	0.12	0.04	0.29	1.53	99.95
		BF VCH2	BF2	68.50	19.05	5.88	2.99	0.41	0.93	0.59	0.12	0.03	0.28	1.47	100.26
		BF VCH3	BF2	68.39	18.55	6.83	2.24	0.51	0.89	0.74	0.10	0.03	0.33	1.29	99.90
Green	Green	BF VP1	BF2	67.20	18.72	6.81	2.23	0.45	1.12	1.31	0.14	0.06	0.24	1.54	99.81
		BF VP2	BF2	66.83	19.55	6.99	2.11	0.39	1.08	1.13	0.13	0.06	0.22	1.72	100.20
		BF VP3	BF2	66.75	18.85	6.45	2.29	0.54	1.08	1.49	0.13	0.10	0.23	1.59	99.48
		BF VP4	BF2	67.29	19.67	6.65	2.28	0.44	1.04	1.11	0.14	0.06	0.26	1.53	100.47
	Dark green	BF VS1	BF2	67.30	19.03	7.45	2.28	0.59	0.90	1.43	0.11	0.16	0.25	1.49	100.99
		BF VS2	BF2	67.38	19.41	6.85	2.20	0.52	1.00	1.33	0.13	0.08	0.24	1.60	100.73
Yellow	Yellow	BF GSO1	BF1	69.84	18.62	6.26	2.03	0.50	0.55	0.48	0.07	0.03	0.28	1.33	99.99
		BF GSO2	BF1	70.05	18.26	5.01	2.15	0.66	0.64	1.41	0.13	0.07	0.41	0.95	99.74
		BF GSO3	BF1	69.76	18.66	4.74	2.24	0.60	0.74	1.46	0.13	0.07	0.34	1.10	99.83
		BF GSO4	BF2	67.86	19.23	6.45	2.38	0.55	0.72	0.92	0.15	0.03	0.22	1.35	99.87
	Yellow green	BF VG1	BF2	67.01	19.77	6.11	2.16	0.53	1.00	1.47	0.13	0.03	0.29	1.37	99.84
Blue	Azure	BF AZ1	BF2	66.33	20.63	6.51	2.36	0.41	1.04	0.97	0.12	0.09	0.33	1.76	100.54
		BF AZ2	BF2	68.31	18.85	7.12	2.15	0.59	0.87	0.85	0.09	0.13	0.32	1.33	100.61
		BF AZ3	BF2	68.25	19.02	6.94	2.14	0.49	0.81	0.87	0.10	0.13	0.34	1.39	100.47
		BF AZ4	BF1	70.62	16.50	6.43	2.64	0.73	0.72	0.95	0.09	0.14	0.36	0.94	100.12
		BF AZ5	BF1	69.19	17.05	7.27	2.37	0.61	0.78	1.12	0.08	0.18	0.37	1.03	100.04
	Blue	BF B1	BF1	70.51	17.12	6.20	2.42	0.70	0.67	0.99	0.11	0.17	0.36	0.89	100.13
White	Grey	BF GR1	BF2	68.98	18.17	6.79	2.20	0.58	0.92	0.73	0.09	0.11	0.37	1.19	100.12
Red	Orange	BF AV1	out	62.45	11.96	12.23	6.48	1.46	2.20	2.35	0.20	0.59	0.27	0.64	100.83
	Brown	BF M1	BF2	67.48	20.36	6.61	2.11	0.48	0.94	1.47	0.13	0.03	0.28	1.46	101.35
		BF M2	BF2	67.73	19.59	6.90	2.24	0.79	0.93	1.48	0.13	0.04	0.25	1.34	101.41
		BF M3	out	64.70	15.11	9.94	2.06	2.63	2.36	1.49	0.13	0.97	0.36	0.82	100.58
		BF M4	BF2	67.49	19.72	6.90	2.23	0.85	0.93	1.46	0.13	0.03	0.27	1.35	101.35
	Red	BF R1	BF1	68.35	16.55	7.74	2.66	0.63	0.71	1.55	0.10	0.12	0.24	1.22	99.87
Colourless	Gold	BF AU1	BF2	68.16	18.75	7.34	2.12	0.49	1.01	0.70	0.11	0.05	0.31	1.30	100.33
		BF AU1cart	BF2	68.54	18.59	7.48	1.99	0.57	1.08	0.75	0.12	0.03	0.31	1.26	100.71
	Colourless	BF TR INC1	BF1	72.53	15.75	7.08	2.37	0.52	0.45	0.35	0.05	0.11	0.12	1.15	100.48
		BF TR INC2	BF2	67.75	19.25	7.15	1.97	0.53	0.94	0.73	0.12	0.03	0.37	1.29	100.12
		BF TR INC3	BF2	68.59	19.61	6.42	2.09	0.39	0.77	0.52	0.10	0.07	0.28	1.61	100.44

Data expressed as weight percent; out: outlier

possible contamination from the crucibles utilised in the secondary working. Unfortunately, discerning the contribution of the base glasses from that of external pollution and/or colouring/opacifying agents is not possible at present, but

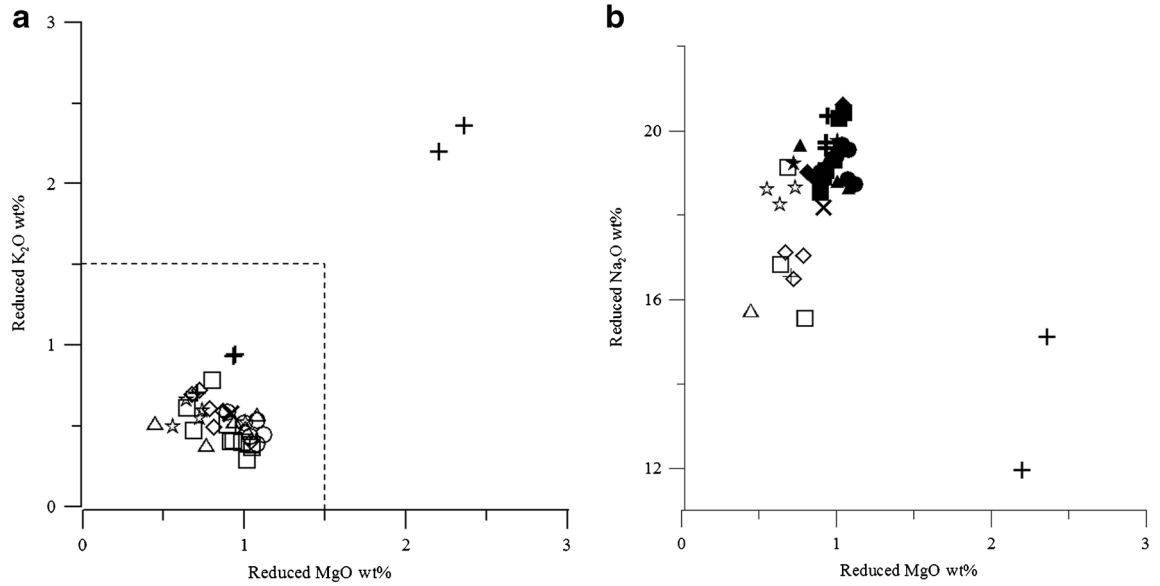

Fig. 1 Binary diagrams. **a** Reduced K_2O vs. reduced MgO. The *broken lines* highlight the compositional fields of natron and plant ash glass (Lilyquist and Brill 1993). **b** Reduced MgO vs. reduced Na_2O. Symbols represent colour macro-groups: turquoise (*square*), green (*circle*), blue (*diamond*), white (*multiplication sign*), yellow (*star*), red (*plus sign*), colourless (*triangle*). Only in (**b**) *empty symbols* represent samples of group BF1 and *solid symbols* BF2

the present chemical data suggest that the BF2 group is obtained by recycling/mixing of various base compositions.

Colouring and opacifying agents

Colour and opacity are the two most important parameters characterising glass mosaic tesserae and are obtained by means of multiple technological choices, which are described here with respect to the colour macro-groups identified in the present assemblage.

The colourless macro-group is composed of one "gold" tessera (BF AU1), which includes gold foil and *cartellina*, and three colourless tesserae (BF TRINC1, 2 and 3) that are interpreted to have been gold tesserae that have lost their metal foil and *cartellina*. The chemical composition of the supporting tessera and *cartellina* of BF AU1, along with those of the three colourless tesserae (Table 1), show that this group is chemically heterogeneous, although the samples are all characterised by iron as the only potential chromophore, along with variable concentrations of manganese and/or antimony, acting as decolourisers. BF TRINC1 is different from the other colourless samples due to its high silica and low soda contents, and it is included in compositional group BF1 (Table 3). In the absence of any intentional decolouriser, it can be considered a "naturally colourless" Roman (see, for instance, group 1b of Jackson 2005). In contrast, tesserae BF AU1, BF TRINC2 and BF TRINC3 are included in group BF2 (Table 3) and are characterised by low concentrations of Mn and Sb (Table 1), reinforcing the hypothesis of recycling (Silvestri et al. 2008). The strict chemical similarity between the two layers (supporting tessera and *cartellina*) in sample BF AU1 (Table 1) indicates that the tessera was produced within a single operation, using the same colourless glass, probably obtained by recycling glasses with different compositions. In addition, the analysis of the gold foil of sample AU1 revealed that it is composed of pure gold (EDS data), which is consistent with the use of an early Roman or a fourth century gold coin as the source of gold (Neri and Verità 2013).

In the blue and turquoise colour macro-groups, the main ionic chromophores detected are cobalt and copper, which are typically found in ancient glass with similar colours (Tite 2003). In the white macro-group, iron, probably unintentionally introduced, is the only colouring element identified.

Cobalt is the principal chromofore detected in the blue (B) and azure (AZ) tesserae, as this element has a very strong colouring power, which prevails over others, such as iron and copper, even at very low concentrations (Gliozzo et al. 2008; Möncke et al. 2014). In the samples BF AZ1 and BF AZ5, cobalt is below the EPMA detection limits, and its presence, expected on the basis of the macroscopic appearance, was checked by means of FORS, which detected a weak cobalt signal (Fig. 2). The cobalt-coloured tesserae also contain copper in low concentrations (ranging from 0.09 to 0.38 wt% as CuO; Table 1) and iron in relatively high concentrations (from 0.83 to 1.1 wt% as Fe_2O_3; Table 1). The simultaneous presence of iron, copper and cobalt is common in glass and is likely related to the cobalt ore (Henderson 1991). However, in the current case, the picture is complicated by the marked heterogeneity of the assemblage: the variable concentrations of these elements and their low degrees of correlation are in accordance with the other chemical and textural

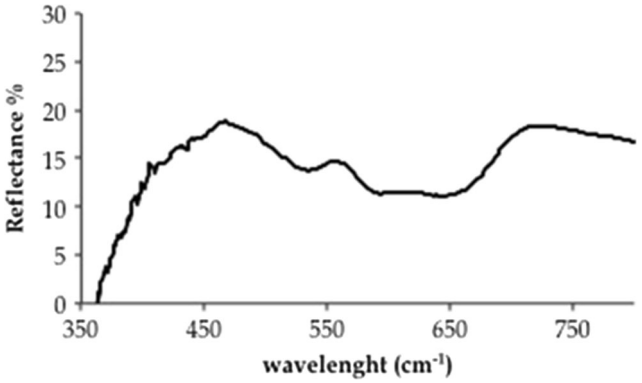

Fig. 2 FORS reflectance spectrum for sample BF AZ1, indicating a weak signal of cobalt in the visible interval. Note the maximum reflectance values at 550 and 625 nm and the minimum reflectance values at 525, 600 and 650 nm (Möncke et al. 2014)

results that support the hypothesis of an assemblage mostly composed of remelted tesserae.

The samples from the turquoise macro-group (chromatic groups BS, TU, AQ, VCH, CE), in which no cobalt was detected by means of EPMA and FORS analyses, are coloured by highly variable concentrations of copper ions (from 0.42 wt% in the pale green BF VCH1 to 4.13 wt% in the turquoise BF-TU1 as CuO; Table 1), suggesting a general proportionality with the intensity of the colour. The use of metalworking scraps as a source of copper in Roman glass is commonly hypothesised (e.g. Mass et al. 1998; Freestone and Stapleton 2003), and the presence of detectable tin in the majority of tesserae (Table 1) supports this hypothesis, although it should be noted that the Cu/Sn ratio is close to 9:1 (typical of ancient bronze) only in BF CE1 and BF VCH2. Therefore, in the tesserae investigated here, it is possible that different sources of copper or different copper alloys were mixed together and that turquoise glasses with different recycling histories were used.

Regarding the opacifiers in the blue, turquoise and white macro-groups, unlike previous reports for Roman and Late Antique opaque glass with comparable colours (e.g. Wypyski and Becker 2005; Gliozzo et al. 2012; Di Bella et al. 2013; Basso et al. 2014; Paynter et al. 2015; Barca et al. 2016), Ca-antimonate is not the most common opacifier, as it was only identified here in five tesserae (BF GR1, BF TU1, BF CE1, BF B1 and BF AZ4). In these tesserae, the crystals are finely dispersed in the glassy matrices (Fig. 3a) and occasionally clustered in small clumps. The dispersed micron-scale crystals (1–5 μm) often exhibit euhedral morphologies that are mostly hexagonal (Fig. 3b), whilst the clusters are generally composed of anhedral and partly reacted compounds and can reach a few millimetres of size (Fig. 3c). The XRD analysis identified the presence of two different crystalline phases of Ca-antimonate: the rhombic ($Ca_2Sb_2O_7$) and the hexagonal ($CaSb_2O_6$) phases. Both phases were detected in all the analysed samples, and the hexagonal phase seems to predominate over the rhombic one, although the experimental XRD conditions do not allow a more precise quantification of the two crystalline phases.

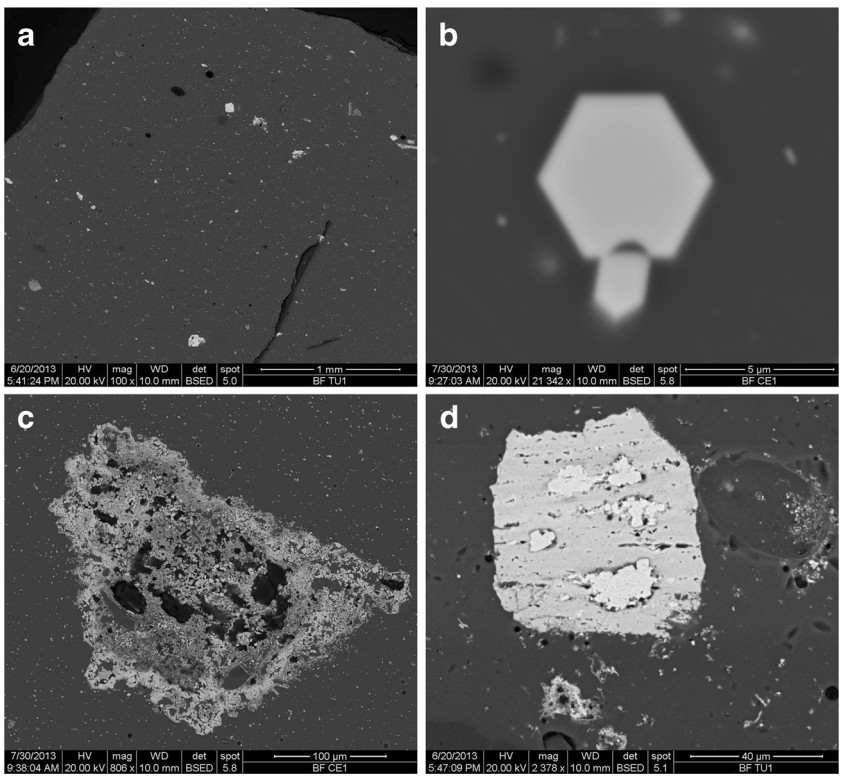

Fig. 3 SEM-BSE images of tesserae opacified with Ca-antimonates: **a** texture of a well-opacified sample (BF TU1); **b** newly formed euhedral crystal showing hexagonal morphology in sample BF CE1; **c** partly melted Ca-antimonate inclusion with newly formed crystals and some relics of quartz (*grey*) and voids (*black*) in sample BF CE1; **d** inclusion of unreacted antimony oxide in sample BF TU1: *brighter areas* are richer in antimony, *grey areas* are richer in oxygen (EDS data)

The presence of the rhombic phase (although reasonable) is uncertain only in BF CE1. The euhedral morphology and the small dimension of the Ca-antimonate crystals suggest in situ crystallisation. However, the presence of presumed relics of Ca-antimonates in BF GR1 and BF CE1 does not fully support this hypothesis. In the opaque turquoise sample BF TU1, some relics of an antimony oxide (EDS data), composed of large anhedral inclusions, were identified, and these inclusions are often surrounded by small, newly formed euhedral Ca-antimonate crystals (Fig. 3d). These specific inclusions and the low calcium content of the glassy matrix (Table 1) suggest that the Ca-antimonate crystallisation was induced by the addition of antimony oxide to the base glass, which also resulted in the depletion of lime in the glassy matrix. The depletion of lime (which is actually very low in BF TU1) has affected the base composition that is not fully interpretable (see previous sub-section for further details).

Some tesserae of the chromatic groups azure (BF AZ1, 2, 3 and 5), pale blue (BF CE2), pale green (BF VCH1, 2 and 3) and aquamarine (BF AQ1 and 2) contain abundant relics of sand, i.e. large, sub-rounded grains of quartz and (to a minor extent) feldspars, and large quantities of gas bubbles trapped in the matrix (Fig. 4a). These tesserae are assigned a difficult interpretation: the sand relics and gas bubbles are interpreted to be intentional opacifiers, based on the very low quantity of other more common opacifiers (such as Ca-antimonate or tin oxide) and the very pale colour of the present samples, which would have not been visible in the absence of some opacifying agent. Other evidence of this opacifying technique in the archaeological record is currently lacking. Quartz as an opacifier is relatively rare (Freestone et al. 1990; Verità 2000; Peake 2014), and glass opacified with bubbles and containing abundant seeds has only been reported for the white and flesh-coloured slabs of the fourth century Thomas Panel (Brill and Whitehouse 1988). Unfortunately, the absence of SEM-BSE images does not allow direct comparisons between those slabs and the samples investigated here. The scarcity of this technique in the archaeometric record may reflect the actual rarity of this technological choice, but it may also be related to the analytical approaches employed: some scholars may have neglected the bubbles or interpreted the seeds as unintentional relics. In addition, large assemblages of glass tesserae were analysed in the past decades by means of bulk chemistry analysis without a preliminary textural analysis, which is fundamental to identifying this specific technique. It is possible that "quartz and bubbles-"opacified glasses were produced in the absence of other opacifiers (such as Ca-antimonate and tin oxide) or, as an alternative, to obtain opalescent tesserae, possibly required for aesthetic needs.

The tesserae with "quartz and bubbles" are all included in the compositional group BF2 and are interpreted as recycled glass. This hypothesis is further supported by the presence of sporadic inclusions of relic cassiterite (in BF AQ1 and BF AZ1) and Ca-antimonates (in BF VCH3, BF AZ1, 2, 3 and 5), suggesting the intermixing of several different glasses, including opaque-coloured mosaic tesserae.

The red macro-group comprises red, brown and orange samples, which in SEM-BSE images appear uniformly opacified by nanometric crystals (Fig. 5a), with apparently cubic (Fig. 5b) or subrounded elongated habits. The identification of the specific crystalline phase involved in the colouring/opacification was conducted by means of XRD analyses, which identified cuprite in the orange sample BF AV1 and metallic copper in the red (BF R1) and the brown tesserae (BF M1, 2, 3 and 4). Both phases crystallised directly in the glassy matrix via an in situ process that required a locally reducing environment. The different types of opacifier are related to the different glassy matrices: the nucleation of cuprite is favoured by high lead and high copper compositions, whilst the precipitation of metallic copper seems to occur with lower copper and low or negligible lead compositions (Freestone 1987; Freestone and Stapleton 2003). In both cases, the locally reducing environment was achieved by means of internal reducing agents. In the tesserae examined here, these internal reducing agents were iron in BF M1, 2 and 4 and iron coupled with antimony, tin and lead in the others. In the three brown tesserae (BF M1, 2 and 4) that contain iron as

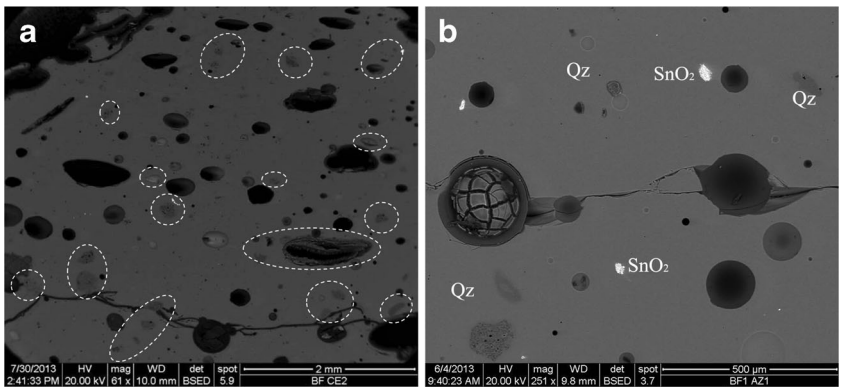

Fig. 4 SEM-BES images of tesserae opacified with quartz and bubbles: sand relics are *medium grey* and gas bubbles are *black*. **a** The quantity and distribution of the inclusions and **b** a detail of the texture of sample BF AZ1. The *white flecks* are tin oxide relics

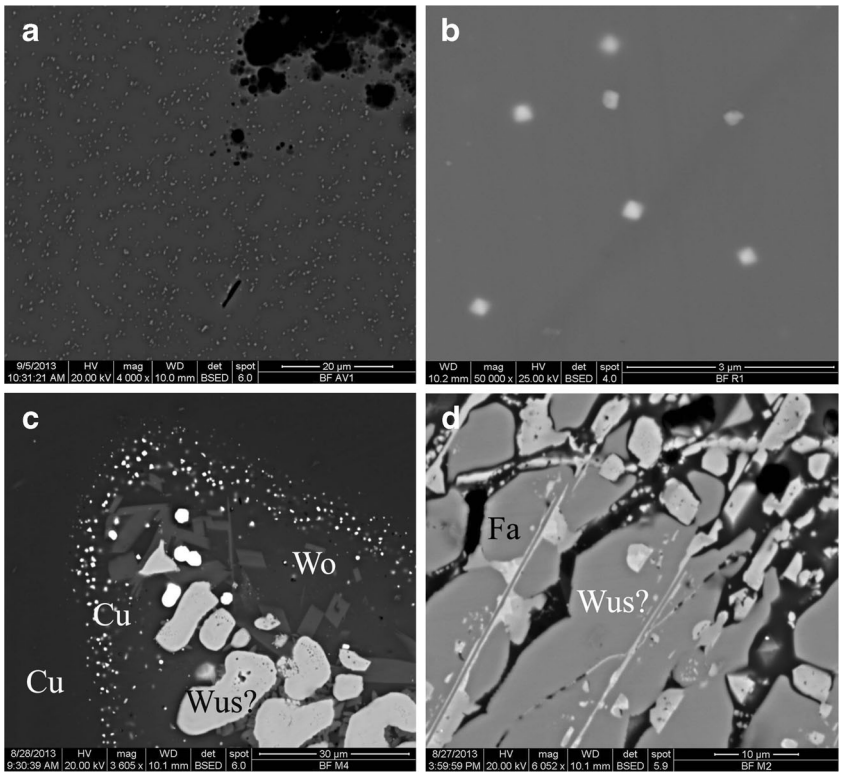

Fig. 5 SEM-BSE images of red tesserae opacified with copper compounds: **a** sample BF AV1, opacified with nanometric cuprite; **b** sample BF R1, opacified with metallic copper, showing euhedral cubic crystals of nanometric dimensions; **c** slag inclusion in sample BF M4: *Wus* = probably wustite, in *brighter grey*, *Wo* = newly formed wollastonite in *darker grey*, *Cu* = metallic copper crystals, in *white*; (**d**) slag inclusion in sample BF M2: *Fa* = fayalite (*medium grey*), *Wus* = probable wustite in *brighter grey*

the only internal reducing agent, aggregates of fayalite (Fe_2SiO_4) and iron oxide (probably wustite, FeO) (Fig. 5c, d) were identified, suggesting that the reducing agent was added in the form of metallurgical slags. The internal reducing power of iron compounds is also evidenced by the presence of copper crystals of larger dimensions surrounding the inclusions (Fig. 5c). Although the use of metallurgical by-products in the colouring of glass is sometimes hypothesised (Mass et al. 1998; Freestone and Stapleton 2003), finding evidence of metallurgical slags in glass is uncommon. To date, previous examples have been identified in Anglo-Saxon red and black beads dated to the fifth to seventh centuries AD (Peake and Freestone 2012 and references therein) and in a glassy layer adhering to a crucible that was used for producing black glass and that was excavated in *Serdica* (Sofia, Bulgaria), probably dating to the Late Roman time (Cholakova and Rehren 2014). The finding of this technology in a mosaic precisely dated to the fourth century AD and located in Italy is in contrast with the hypothesis that this technique was typical of north-western Europe during the Middle Ages (Peake and Freestone, 2012) and highlights the existence of cross-craft interactions between metal and glass-working.

Finally, it should be noted that in the presumed plant ash tesserae (i.e. samples BF M3 and BF AV1), in addition to iron, tin, antimony and lead in different concentrations, the probable use of charcoal and fuel ashes as further reducing agents cannot be excluded, and these agents may have influenced the chemical composition of the glassy matrix of the above tesserae, as discussed in the previous sub-section.

The green and yellow colour macro-groups both feature the use of a yellow opacifying phase embedded in a glassy matrix, which is colourless in the yellow tesserae and copper coloured in the green tesserae. An exception is the translucent dark green tessera, BF VS2, which does not have any opacifier. This sample, coloured by copper, also contains high zinc contents and lacks tin and antimony (Table 1), suggesting that brass scraps were used as the colouring agent. Amongst the opaque yellow and green tesserae, two different opacifiers were detected: Pb-antimonate and Pb-stannate. In detail, Pb-antimonate was identified in three of the four yellow samples (BF GSO1, 2 and 3), whilst Pb-stannate was identified in one of the yellow (BF GSO4), in the yellow green (BF VG1), in all the green (BF VP1, 2, 3 and 4) and one of the dark green samples (BF VS2).

The textural features of the green and yellow tesserae are very similar, with anhedral crystals of 1–2 μm unevenly distributed in a zoned glassy matrix, occasionally clustered in small clumps or "chains" and concentrated in bands with higher average atomic numbers (Fig. 6). The XRD analyses identified Pb-antimonate in the form of anhydrous, synthetic bindheimite ($Pb_2Sb_2O_7$) in the samples BF GSO1 and 3. The opacifiers in BF GSO2 were checked only by means of SEM-EDS due to the small dimensions of the sample. Conversely, the bulk XRD analysis performed on a whole sample proved to be not efficient at distinguishing Pb-stannate from other

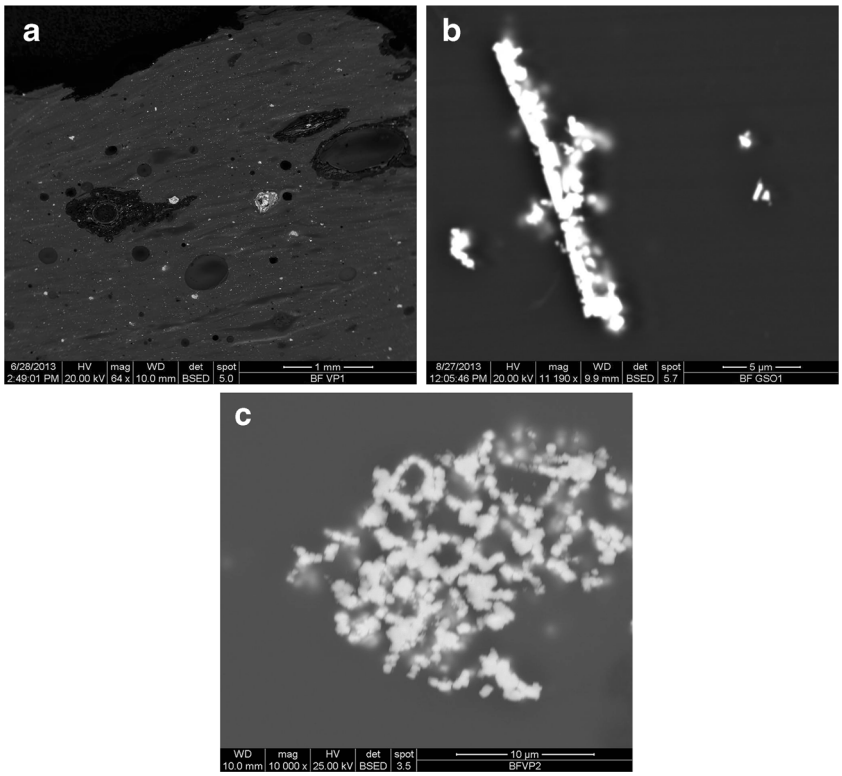

Fig. 6 SEM-BSE image of tesserae opacified with lead-antimonate or lead-stannate: **a** sample BF VP1, opacified with Pb-stannate showing the uneven distribution of the crystals and the presence of clusters; **b** detailed image of a cluster of Pb-antimonate in sample BF GSO1, showing the subhedral and anhedral habits of the crystals; **c** a small clump of Pb-stannate in the sample BF VP1, showing the subhedral and anhedral habits of the crystals

phases with similar structures (i.e. other cubic pyrochlores with the general formula $A_2B_2O_{6.5}$ containing variable amounts of antimony or tin (Cascales et al. 1986)). Therefore, to determine the ratio between tin and antimony, which allows us to discriminate amongst Pb-antimonate, Pb-stannate and Pb-Sn antimonate, preliminary quantitative analyses were performed by means of EPMA, and the marked predominance of tin and lead was observed, confirming the presence of Pb-stannate in the yellow tesserae (BF GSO4), in the yellow green (BF VG1) and in all the opaque tesserae of the green colour macro-group.

The textural characteristics of tesserae with Pb-antimonate or Pb-stannate, as shown by the SEM-BSE analyses (Fig. 6), suggest that the opacifiers in both cases were synthesised ex situ and added to the molten glass in a very quick process. The use of such a method has been supported for Roman and Late Roman glassmaking by experimental works (Tite et al. 2008; Molina et al. 2014). Both compounds are unstable at high temperatures, but their stability is enhanced when they are synthesised ex situ. In the case of Pb-stannate, the presence of silica, confirmed by means of the EPMA, suggests that this compound was produced with the *anime* method (Moretti and Hreglich 1984), which was also hypothesised on the basis of previous analytical and experimental works for similar compounds (Rooksby 1964; Heck et al. 2003; Tite et al. 2008).

In general, Pb-antimonate is a very common yellow opacifier in pre-Roman and Roman glassmaking until the fourth century AD, when it was replaced by Pb-stannate (Lahlil et al. 2009; Lahlil et al. 2011; Molina et al. 2014). Pb-stannate is rare before the fourth century AD. Apart from some British and French beads dated to the second to first centuries BC, the use of tin-based opacifiers is documented in India starting in the first century AD (Tite et al. 2008) and in some yellow slabs dated to the first century AD in the Gorga collection in Rome (Verità et al. 2013). One of the possible explanations for the introduction of this compound in the Roman Empire may be the documented trades amongst India, Egypt and Rome (Tite et al. 2008); nevertheless, such early use in Rome is an exception with no other documented instances before the fourth century AD until now. The presence of Pb-stannate in the current assemblage may be considered a sign of the rapid introduction of this new opacifying technology in Aquileia, further reinforcing the hypothesis of a Late Antique production.

Conclusions

The archaeometric study of the glass tesserae from the mosaic of the House of the Wounded Animals in Aquileia has provided deep insights into the glassmaking technology of the fourth century AD.

The variety of colours and techniques employed in this mosaic is remarkable, and no clear link was identified amongst specific technological solutions and groups of mosaicists or portion of the mosaic, suggesting that the different

groups of workers, that worked independently, had access to the same stock of tesserae.

The assemblage is heterogeneous, and each chromatic group is composed of tesserae produced with different base glasses and colouring/opacifying techniques, suggesting diverse supplies.

In particular, tesserae showing strict chemical and technological links with the early Roman tradition are employed alongside a large number of tesserae characterised by "modern" technological solutions, evidencing the complexity of the glassmaking industry in the period considered here.

The truly "Roman" tesserae identified here were likely obtained from Roman glass cakes or by re-using the tesserae from pre-existing mosaics, which were certainly still readily available in Aquileia. In contrast, given the specific compositional and textural fingerprints of the "modern" tesserae, it is possible to hypothesise that secondary production occurred in the fourth century, possibly for the purpose of creating the Wounded Animals mosaic, although this assertion cannot be proved. The colouring and opacification processes employed in the production of these tesserae are relatively simple: the green and yellow were produced by adding a ready pigment (Pb-stannate) to a molten glass, and the blue and turquoise were probably produced by mixing old tesserae and colourless glass with the addition of additional quartz sand, which, together with gas bubbles, acted as a weak opacifier.

The contemporary presence of antimony- and tin-based opacifiers in the same mosaic is of particular interest, suggesting both the prompt acceptance of technological innovations and the persistence of the Roman traditions in the city of Aquileia. The ready introduction of the tin-based opacification confirms the role of Aquileia as a cultural and economic outpost in the Antique and Late Antique Mediterranean trade. In addition, the use of Pb-stannate together with uncommon opacifiers (quartz and bubbles) as substitutes for Ca-antimonate may reflect the well-documented decrease in the availability of antimony in the fourth century, which likely made it less accessible and/or more costly.

In conclusion, the technological variety identified in the mosaic of the Wounded Animals mirrors the political, economic and cultural complexity of the fourth century AD, which is confirmed to be a period of transition between the Roman and the early Christian/Byzantine periods.

Acknowledgments The authors are grateful to *Soprintendenza per i Beni Archeologici del Friuli Venezia Giulia* for authorising the present study; Dr. P. Guerriero (CNR-ICMATE, Padova, Italy), Prof. M. Vandini and T. Chinni (University of Bologna, Italy) for the use of SEM-EDS; R. Carampin (CNR-IGG Padova, Italy) for the EPMA analysis; Prof. F. Nestola and F. Zorzi (University of Padova, Italy) for XRD analyses; Prof. G. Molin (University of Padova, Italy) for his advice and useful discussion; Prof. M. Salvadori (University of Padova, Italy) for her archaeological support; and James Peake (Bonhams, UK) for useful discussion and cooperation.

Financial support was provided by the project PRAT 2012 of the University of Padova, named "Crystals in ancient glass mosaics as indicators of raw materials and production technologies" (grant number: CPDA127550).

References

Angel RJ, Nestola F (2016) A century of mineral structures: how well do we know them? Am Mineral 101:1036–1045

Barca D, Basso E, Bersani D et al (2016) Vitreous tesserae from the calidarium mosaics of the *Villa dei Quintili*, Rome. Chemical composition and production technology. Microchem J 124:726–735

Basso E, Invernizzi C, Malagodi M et al (2014) Characterization of colorants and opacifiers in Roman glass mosaic tesserae through spectroscopic and spectrometric techniques. J Raman Spectrosc 45:238–245

Bertacchi L (1963) Nuovi mosaici figurati ad Aquileia. Aquil Nostra 34: 19–42

Boschetti C, Leonelli C, Macchiarola M et al (2008) Early evidences of vitreous materials in Roman mosaics from Italy: an archaeological and archaeometric integrated study. J Cult Herit 9:e21–e26

Brill RH, Whitehouse D (1988) The Thomas panel. J Glass Stud 30:34–50

Bueno M, Centola V (2014) Le domus di Aquileia e le loro evoluzioni architettonico-funzionali in età tardoantica: i casi delle domus delle Bestie Ferite e di Tito Macro presso i Fondi Ex-Cossar. In: Cuscito G (ed) Costantino il Grande a 1700 anni dall' "Editto di Milano". Editreg, Trieste, pp 317–334

Bueno M, Mantovani V, Novello M (2012) Lo scavo della casa delle Bestie Ferite. In: Bonetto J, Salvadori M (eds) L'architettura privata ad Aquileia in età romana, Atti del Convegno di Studio (Padova, 21–22 Febbraio 2011). Padova University Press, Padova, pp 77–100

Cable M, Smedley JM (1987) The replication of an opaque red glass from Nimrud. In: Bimson M, Freestone IC (eds) Early vitreous materials. British Museum Occasional paper 56, London, pp 151–164

Cascales C, Alonso JA, Rasines I (1986) New pyrochlores $Pb_2(MSb)O_{6.5}$ (M equals Ti, Zr, Sn, Hf). J Mater Sci Lett 5:675–677

Cholakova A, Rehren T (2014) Producing black glass during the Roman period—notes on a crucible fragment from Serdica, Bulgaria. In: Proceedings of the 39th International Symposium for Archaeometry. pp 261–267

Di Bella M, Quartieri S, Sabatino G et al (2013) The glass mosaics tesserae of "Villa del Casale" (Piazza Armerina, Italy): a multitechnique archaeometric study. Archaeol Anthropol Sci 6:345–362

Freestone IC (2008) Pliny on Roman glassmaking. In: Martinon-Torres M, Rehren T (eds) Archaeology, history and science. Integrating approaches to ancient materials. UCL Institute of Archaeology Publications, Oxford, pp 77–100

Freestone IC (1994) Chemical analysis of raw glass fragments. In: Hurst HR (ed) Excavation at Carthage, The Circular Harbour, North Side. the Site and Finds Other than Pottery. Vol II. Oxford University Press, Oxford, p 290

Freestone IC (1987) Composition and microstructure of copper opaque red glass. In: Bimson M, Freestone IC (eds) Early vitreous material, vol 56, British Museum Occasional Paper. British Museum, London, pp 173–191

Freestone IC, Bimson M, Buckton D (1990) Compositional categories of Byzantine glass tesserae. In: Annales du 11e Congrès de l'Association International pour l'Histoire du Verre (AIHV), Amsterdam, pp 271–280

Freestone IC, Gorin-Rosen Y, Hughes MJ (2000) Primary glass from Israel and the production of glass in Late Antiquity and the Early Islamic Period. In: Nenna MD (ed) La Route du Verre. Ateliers

Primaires et Secondaires du Second Millènaire av. JC au Moyen Age. Maison de l'Orient Mediterranéen, Lyon, pp 65–83

Freestone IC, Stapleton CP (2003) The production of red glass and enamel in the Late Iron Age, Roman and Byzantine periods. In: Entwistle C (ed) Through a glass brightly: studies in Byzantine and Medieval art and archaeology; presented to David Buckton. Oxbow Books, Oxford, pp 142–154

Gliozzo E, Santagostino Barbone A, Dacapito F et al (2008) The sectilia panels of Faragola (Ascoli Satriano, Italy): a multi-analytical study of the red, orange and yellow glass slabs. Archaeometry 50:451–473

Gliozzo E, Santagostino Barbone A, Turchiano M et al (2012) The coloured tesserae decorating the vaults of the Faragola *balneum* (Ascoli Satriano, Foggia, southern Italy). Archaeometry 54:311–331

Heck M, Rehren T, Hoffmann P (2003) The production of lead-tin yellow at Merovingian Schleitheim (Switzerland). Archaeometry 45:33–44

Henderson J (1991) Technological characteristics of Roman enamels. Jewel Stud 5:65–76

Jackson CM (2005) Making colourless glass in the Roman period. Archaeometry 47:763–780

Lahlil S, Biron I, Galoisy L, Morin G (2009) Technological processes to produce antimonate opacified glass throughout history. In: Annales du 17e Congrés l'Association International pour l'Histoire du Verre (AIHV), pp 571–578

Lahlil S, Cotte M, Biron I et al (2011) Synthesizing lead antimonate in ancient and modern opaque glass. J Anal At Spectrom 26:1040–1050

Lilyquist C, Brill RH (1993) Studies in early Egyptian glass. Metropolitan Museum of Art, New York

Mass JL, Stone RE, Wypyski MT (1998) The mineralogical and metallurgical origins of Roman opaque colored glasses. In: Kingery WD, McCray P (eds) The prehistory and history of glassmaking technology, ceramics and civilization. The American Ceramic Society, Ohio, pp 121–144

Molina G, Odin GP, Pradell T et al (2014) Production technology and replication of lead antimonate yellow glass from New Kingdom Egypt and the Roman Empire. J Archaeol Sci 41:171–184

Möncke D, Papageorgiou M, Winterstein-Beckmann A, Zacharias N, (2014) Roman glasses coloured by dissolved transition metal ions: redox-reactions, optical spectroscopy and ligand field theory. J Archaeol Sci 46:23–36

Moretti C, Hreglich S (1984) Opacification and colouring of glass by the use of "anime". Glas Technol 25:277–282

Nenna MD, Picon M, Vichy M (2000) Ateliers primaires et secondaires en Ègypt à l'époque gréco-romaine. In: Nenna MD (ed) La Route du Verre: Atelieres primaires et secondaires du second millinaire av. J.-C. au Moyen-Age. Maison de l'Orient Méditerranéen, Lyon, pp 97–112

Neri E, Verità M (2013) Glass and metal analyses of gold leaf tesserae from 1st to 9th century mosaics. A contribution to technological and chronological knowledge. J Archaeol Sci 40:4596–4606

Nestola F, Burnham AD, Peruzzo L, et al. (2016) Tetragonal Almandine-Pyrope Phase, TAPP: finally a name for it, the new mineral jeffbenite. Mineral Mag. doi: 10.1180/minmag.2016.080.059

Newton R, Davison S (1989) Historical development of glass. In: Conservation of glass. Butterworth-Heinemann, Oxford, pp 18–53

Paynter S (2008) Experiments in the reconstruction of Roman wood-fired glassworking furnaces: waste products and their formation processes. J Glass Stud 50:271–290

Paynter S, Kearns T, Cool H, Chenery S (2015) Roman coloured glass in the Western provinces: the glass cakes and tesserae from West Clacton in England. J Archaeol Sci 62:66–81

Peake JRN (2014) Early Anglo-Saxon glass beads: composition and origins based on the finds from RAF Lakenheat. Cardiff University, Suffolk

Peake JRN, Freestone IC (2012) Cross-craft interactions between metal and glass working: slag additions to early Anglo-Saxon red glass. In: Thienpont H, Meulebroeck W, Nys K, Vanclooster D (eds) Integrated approaches to the study of historical glass. SPIE Proceedings, Brussels

Rooksby HP (1964) A yellow cubic lead tin oxide opacifier in ancient glasses. Phys Chem Glas 5:20–25

Salvadori M, Boschetti C (2014) "Lavorare stanca": la disorganizzazione di una bottega di mosaicisti in età tardoantica. Il caso del mosaico delle Bestie Ferite. In: Cuscito G (ed) Costantino il Grande a 1700 anni dall' "Editto di Milano". Editreg, Trieste, pp 335–350

Schibille N, Degryse P, Corremans M, Specht CG (2012) Chemical characterisation of glass mosaic tesserae from sixth-century Sagalassos (south-west Turkey): chronology and production techniques. J Archaeol Sci 39:1480–1492

Shortland AJ (2002) The use and origin of antimonate colorants in early Egyptian glass. Archaeometry 44:517–530

Shortland AJ, Schachner L, Freestone IC, Tite M (2006) Natron as a flux in the early vitreous materials industry: sources, beginnings and reasons for decline. J Archaeol Sci 33:521–530

Silvestri A, Molin G, Salviulo G (2008) The colourless glass of Iulia Felix. J Archaeol Sci 35:331–341

Silvestri A, Tonietto S, Molin G (2011) The palaeo-Christian glass mosaic of St. Prosdocimus (Padova, Italy): archaeometric characterisation of "gold" tesserae. J Archaeol Sci 38:3402–3414

Silvestri A, Tonietto S, Molin G, Guerriero P (2015) Multi-methodological study of palaeo-Christian glass mosaic tesserae of St. Maria Mater Domini (Vicenza, Italy). Eur J Mineral 27:225–245

Silvestri A, Tonietto S, Molin G, Guerriero P (2014) The palaeo-Christian glass mosaic of St. Prosdocimus (Padova, Italy): archaeometric characterisation of tesserae with copper- or tin-based opacifiers. J Archaeol Sci 42:51–67

Tite M (2003) Production technology for copper-and cobalt-blue vitreous materials from the New Kingdom site of Amarna—a reappraisal. Archaeometry 2:285–312

Tite M, Pradell T, Shortland AJ (2008) Discovery, production and use of tin-based opacifiers in glasses, enamels and glazes from the late iron age onwards: a reassessment. Archaeometry 50:67–84

Verità M (2000) Tecniche di fabbricazione dei materiali musivi vitrei. Indagini chimiche e mineralogiche. In: Borsook E, Gioffredi Superbi F, Pagliarulo G (eds) Medieval mosaics. Light,color, materials. Silvana Editoriale, Cinisello Balsamo (Milano), pp 47–64

Verità M, Maggetti M, Saguì L, Santopadre P (2013) Colors of Roman glass: an investigation of the yellow sectilia in the Gorga collection. J Glass Stud 55:39–52

Wypyski MT, Becker L (2005) Glassmaking technology at Antioch. In: Becker L, Kondoleon C (eds) The arts of Antioch. Worchester Art Museum, Worchester, pp 116–175